DISPLACEMENT MECHANISMS IN SINGLE AND MULTIPLE PORES FROM LATTICE BOLTZMANN SIMULATIONS AND MICRO-FLUIDIC EXPERIMENTS

Edo S. Boek[†*], Jianhui Yang[†], Emily M. Chapman[†] and John P. Crawshaw[†]

[†] Department of Chemical Engineering, Qatar Carbonates and Carbon Storage Research Centre
Imperial College London, South Kensington Campus, London SW7 2AZ, United Kingdom
e-mail: e.boek@imperial.ac.uk, web page: http://www.imperial.ac.uk/

This paper was prepared for presentation at the International Symposium of the Society of Core Analysts held in Avignon, France, 8-11 September, 2014

ABSTRACT

We have studied displacement mechanisms of immiscible fluids in micro-fluidic models with designs ranging from simple pore junctions to a pore from a rock thin section. For this purpose, we have developed a lattice-Boltzmann (LB) model to study the multi-phase flow processes in direct comparison with experimental results in purpose-built micro-fluidic geometries. In this paper, we will focus on the LB simulations, in direct comparison with the experiments. First, we study quasi-static drainage and imbibition processes in single junctions and observe good agreement with Young-Laplace capillary filling rules. However, for dynamic imbibition, we observe that the sequence of pore filling is determined by local pore geometry rather than the Young-Laplace law. The LB simulation results are in good agreement with the micro-fluidic experimental observations. Having validated the validity of the LB code for displacement mechanisms in single pores, we extend our calculations to multiple-pore displacement in pore space images of real rock samples obtained from micro–computed tomography (micro-CT) scans. We observe capillary pressure and relative permeability curves in good agreement with experiments.

INTRODUCTION

In order to meet current energy demands and address climate change issues, there is a pressing need to enhance our fundamental understanding of Enhanced Oil Recovery (EOR) and Carbon Capture and Utilised Storage (CCUS) processes. To select the most efficient method at the reservoir scale, we require detailed knowledge of multiphase flow and physical chemistry in porous media. Typically, core flood tests are carried out to address these problems. However, core flood test are time-consuming and expensive; also they are destructive, so that the multitude of experimental control parameters cannot be investigated independently under the same conditions on the same core. For this reason, Digital Rock Physics (DRP) approaches are currently increasingly being considered as a

complement to experimental studies. For many EOR and CCUS processes, the efficiency is determined by displacement mechanisms at the pore scale. The DRP approach offers the possibility to study pore scale displacement mechanisms using computer simulation methods. Using DRP methods, we may predict flow and transport directly on 3D digital pore space images obtained from e.g. micro-CT scanning. This can be repeated for a wide range of reservoir P and T conditions, flow rates and fluid compositions, using the same digital rock sample. It should be noted that DRP methods do not replace but complement experiments. The methods under consideration, including direct Navier-Stokes solvers, Lattice-Boltzmann (LB) and Direct Hydrodynamic (DHD) simulations, are still under development and need to be validated thoroughly. For this purpose, we report here an investigation of displacement mechanisms in single pore junctions, using micro-fluidic experiments in direct comparison with LB computer simulations.

For the purpose of both CO_2 storage in and EOR from rock formations, it is important to consider the injection of a non-wetting fluid (drainage) followed by spontaneous imbibition of a wetting fluid. These processes determine the initial and residual saturations respectively. Lenormand et al. [1] investigated these fluid displacement mechanisms in resin etched networks of straight channels, varying in width with multiple menisci displacement processes identified. In the case of two immiscible fluids (oil – air), Lenormand et al. [1] illustrated that the Young-Laplace Equation was sufficient to describe all menisci displacement mechanisms:

$$P_C = P_{NWP} - P_{WP} = 2\gamma \cos\theta\left(\frac{1}{h} + \frac{1}{w}\right) \quad (1)$$

where P_c is the capillary pressure, γ is the interfacial tension, θ the contact angle and h and w the height and width of the channel. Eqn. (1) is used to calculate drainage and imbibition displacements, based on the difference between the pressure of non-wetting (P_{NWP}) and wetting phase (P_{WP}). Here we consider pore junctions with unequal channel widths. For primary drainage, where the non-wetting phase is injected into a medium saturated with wetting phase, we then expect the non-wetting phase to select the channel with the lowest capillary entry pressure first, i.e. the widest channel. For imbibition, where the wetting phase is injected into a porous medium initially filled with non-wetting phase, the wetting phase should enter the narrowest channel with the highest capillary pressure. During imbibition, a proportion of the non-wetting phase can become trapped by snap-off as a displacement mechanism. [2]

This work aims to find a comprehensive solution to the question of whether the capillary pressure filling rules used in network modelling are actually observed in single junction displacement experiments and direct simulations. We report experiments and LB simulations to study drainage and spontaneous imbibition in single junction micro-models, as a model for EOR from and CO_2 storage in porous media. Based on this validation, we extend our simulations to immiscible displacement in digital rock cores and calculate capillary pressure and relative permeability in comparison with experiments.

EXPERIMENTAL METHODOLOGY

Three micro-models with an etch depth of 50 μm were designed to study fluid flow in single pore junctions. The models vary in complexity, ranging from simple square pores with equal arms and unequal arms, to a single pore structure taken from an actual Berea sandstone. [3] The patterns with typical scales are shown in Figure 1. The oil-wetting micro-models were fabricated in Poly[methyl methacrylate] (PMMA) by Epigem Ltd. We used decane and air as wetting and non-wetting phases respectively. A Zeiss inverted microscope (AXIP Observer A1.M) was used to capture still images and the displacement process was captured by a high speed video microscope (FastCam MC2.1, Photron) with a maximum frame rate of 10,000 frames per second (fps) and a resolution of 512x512 up to a recording setting of 2,000 fps. For more details, we refer to [4, 5].

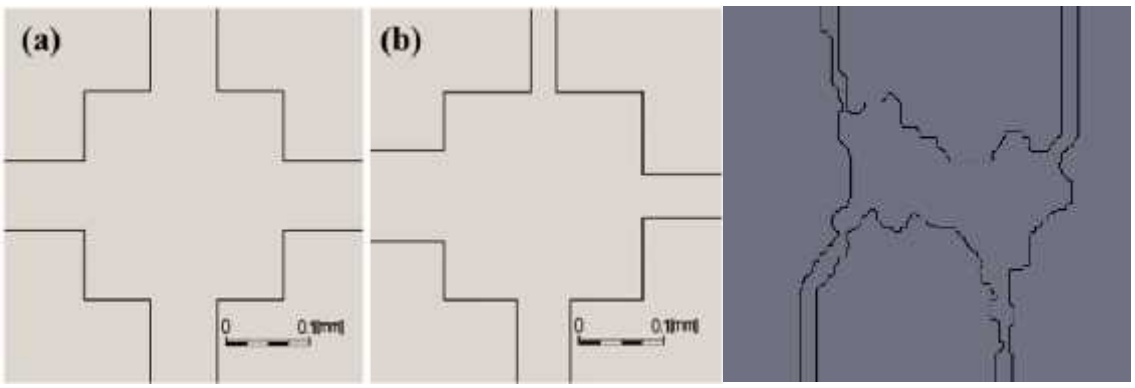

Figure 1: Single Junction Designs with pore body width p and arm widths a: a) p = 160 μm and a = 80 μm; b) p = 235 μm and 27 μm < a < 80 μm; c) Berea pore with narrowest constrictions in top left and bottom right arms of 15 and 22 μm respectively.

LATTICE BOLTZMANN METHOD

In parallel to the experiments, we have carried out immiscible fluid flow calculations, using the lattice Boltzmann (LB) method. For the immiscible fluids, we use the colour gradient (CG) multi-component model. The theoretical background of the LB simulator and CG model are explained in detail in [6]. In the past decade, the LB method has evolved into an alternative and powerful numerical scheme for simulating fluid flow, particularly for problems involving interfacial dynamics and complex boundaries. Unlike traditional Computational Fluid Dynamics (CFD) methods, which solve the conservation equations of macroscopic properties numerically, the LB method is based on micro/mesoscopic models and kinetic equations. The basic idea of the LB method is to create simplified kinetic models that include the essential physics of micro/mesoscopic processes so that the macroscopic averaged properties obey the desired macroscopic equations. The incompressible Navier-Stokes (NS) equations can be obtained in the nearly incompressible limit of the LB method. The pressure in LB models is calculated

using an equation of state, while in the conventional simulation of the incompressible NS equations, the Poisson equation has to be solved, often leading to numerical problems. The underlying kinetic equation provides many advantages, including clear physical pictures, easy implementation of boundary conditions, and fully parallel algorithms. We have implemented our LB code using parallel central processing unit (CPU) and graphics processing unit (GPU) algorithms, enabling us to tackle flow problems in large computational domains on reasonable time scales. For the boundary conditions, we use the simple half-way bounce back scheme, which offers second order accuracy and conserves mass of all components. To simulate spontaneous imbibition, a modification on the geometry was performed. We took the micro-model with a square pore in the center as an example to show the initial configuration of the simulation. This configuration is shown in Figure **2**. A big reservoir which connects the top three channels was built for both phases at the bottom; periodic boundary conditions were applied in X, Y and Z direction.

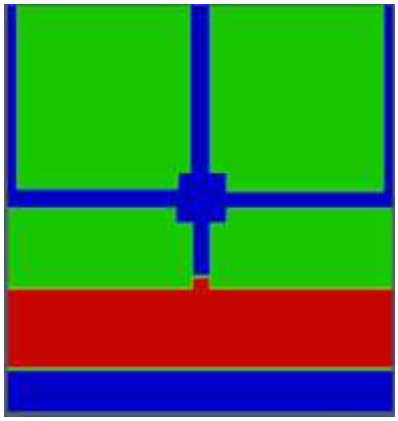

Figure 2: The initial configuration for multi-component simulation, where green represents the solid; the colours blue and red represent air and decane respectively.

For the main displacement process of two-component flow in micro-models, the Reynolds number is very small (< 0.01), so that inertial effects are negligible. The density of both phases in the simulation was set as equal. We define the capillary number *Ca,* representing the relative effect of viscous forces and surface tension as

$$Ca = \frac{u_w \mu_w}{\sigma}, \tag{2}$$

where u_w and μ_w are the Darcy velocity and dynamic viscosity of the wetting phase respectively. σ is the value of surface tension, set to 10^{-2} in lattice units [l.u.] for all simulations. We use a low viscosity ratio of 10 in the simulation rather than the real decane/air system viscosity ratio of 50. This is justified because the typical capillary number for the flow in micro-models is of the order of 10^{-5} which means that capillary

forces dominate the displacement process. Therefore a ratio of 10 or even lower should be sufficient to reproduce the main physical processes [7]. The contact angle is set to 30°, which is consistent with oil-water contact angles in water-wet rocks. For the detailed implementation of the contact angle in LB simulations, we refer to [8].

The initial distribution of decane and air is shown in Figure **2**. Because the micro-model is oil-wet, the decane will spontaneously imbibe into the model due to the capillary pressure. A video of the process was captured by the high-speed camera for comparison with the LB simulations. It is worth noting that all the simulations were performed in 3D in order to recover the experiments.

SIMULATION RESULTS IN COMPARISON WITH EXPERIMENT

Primary Drainage

First, the primary drainage process was studied. The non-wetting fluid was forced to enter the single square pore model with unequal arms from the top-right channel. A body force of 10^{-5} [l.u.] was imposed along the entry channel direction to mimic the pressure gradient in the experiments. Imposing a body force can be considered equivalent to imposing a pressure gradient [9], following Darcy's law

$$J = -\frac{K}{\mu}(\nabla P - \rho g) \tag{3}$$

where J is the flow rate per unit area of cross section (flux), K is the permeability, ∇P is the pressure drop, ρ is the fluid density, g is body force (for example gravity), and μ is the dynamic viscosity of the fluid (related to the kinematic viscosity by $\mu = \nu\rho$).

In Figure **3** we show snapshots for the experimental drainage process (left) in direct comparison with LB simulations (right). The non-wetting fluid enters through the top-left channel and subsequently enters the opposite channel, which has the largest width. The filling sequence is in agreement with the capillary filling law as the channel with the lowest capillary pressure is filled first. The LB simulation results are in good agreement with the displacement sequence observed in the micro-model. Figure **3** shows also that the curvature of the interface and details of the fluid distributions observed in the experiment are well matched by the simulation results. In detail, the two bubbles generated by snap-off in the bottom-left and bottom-right corner of the pore, are captured by the LB simulation. However, the volume of the bubbles in the simulation is slightly bigger than that in experiments; this deviation may be caused by the neglect of density contrast and compressibility of the air/decane system. However, we believe that the fundamental physics of the displacement process, as shown in the experiment, is reproduced well by the simulations.

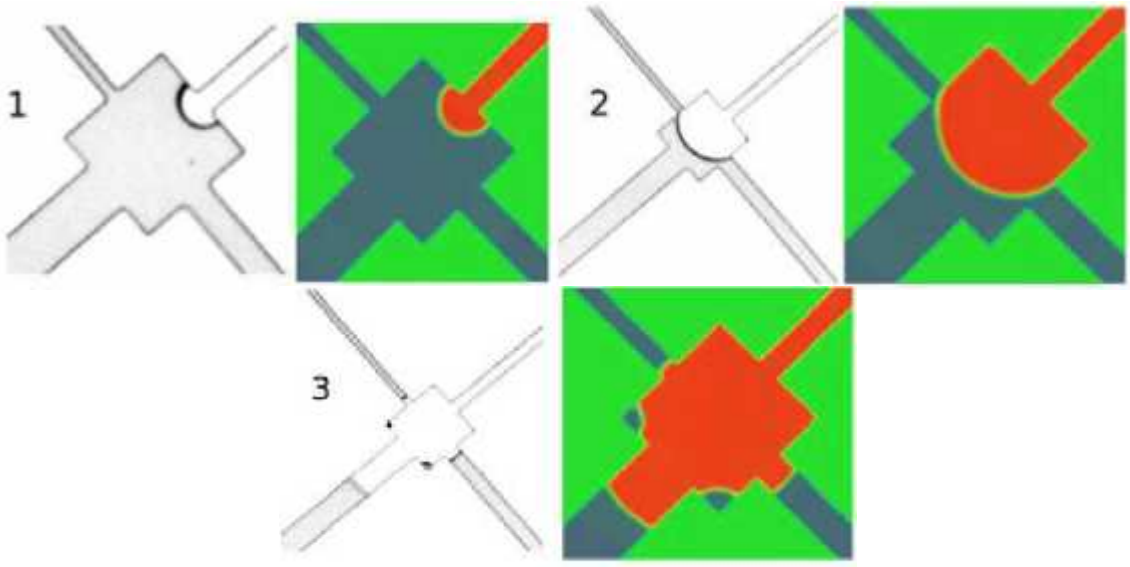

Figure 3: Snapshots of primary drainage of non-wetting fluid in a single junction micro-model for experiments (left) in direct comparison with LB simulations (right).

Imbibition

First, we have investigated quasi-static imbibition. In this case, the micro-model was connected to a reservoir filled with the wetting phase. P_W was then gradually increased by raising the height of the reservoir. This was done for experimental micro-models with equal and unequal channel widths. In both cases, the critical pressure of the pore filling events calculated from the Young-Laplace equation is very close to the experimentally determined critical pressures [5]. For more details on the quasi-static imbibition experiments, we refer to [5]. In this manuscript, we will focus on dynamic spontaneous imbibition. Dynamic displacement was achieved by placing a droplet of the wetting phase over an inlet port which then spontaneously imbibes into the model. Results for the single junction micro-model with unequal channel widths for experiments and corresponding LB simulations are shown in Figure 4. In addition, we consider a micro-model of a pore taken from a thin section of a Berea sandstone [3] and present the results in

Figure 5. The snapshots are taken from the top of the micro-models. The black-white snapshots are experimental data, where the light grey and dark grey represent decane and air respectively and the interface is shown in black. The LB simulations are shown in colour: the red, blue and green represent decane, air and solid PMMA base respectively.

In Figure **4**, we show experimental and simulation snapshots for the dynamic spontaneous imbibition in a square junction with unequal channel widths. We observe that, after initial imbibition in the bottom right corner, the second channel filled is the top right channel. This is *not* the smallest channel with the highest capillary entry pressure, as we would

expect based on Eqn. (1). In contrast, we observe that the the nearest channel is filled first. The LB simulations are in close agreement with the experiments.

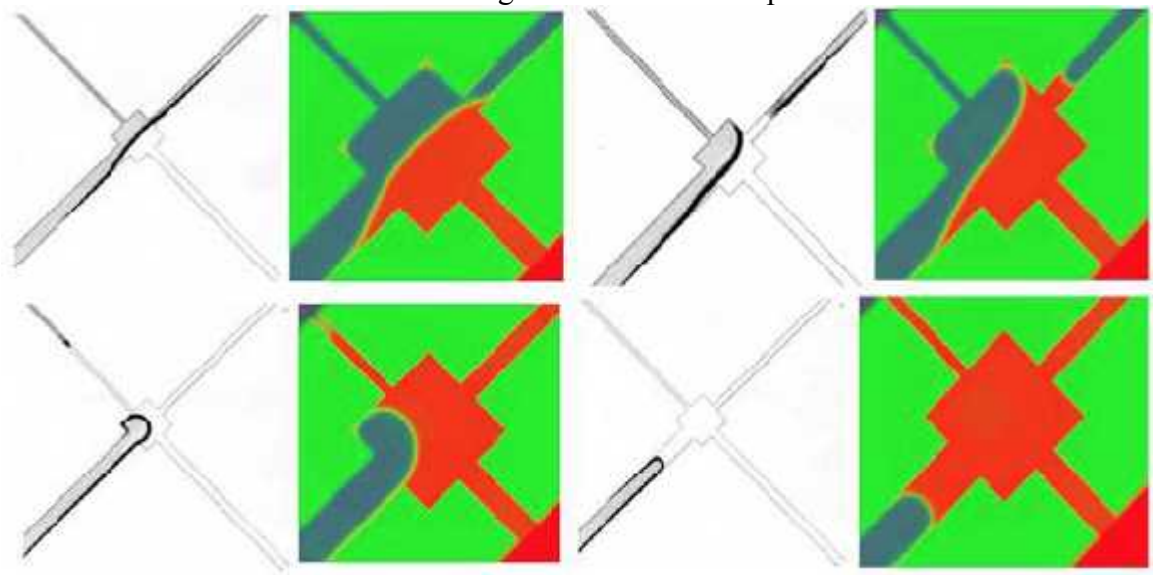

Figure 4: Sequential snapshots of spontaneous imbibition of decane in a single junction micro-model with unequal arms.

To check our observations, we consider dynamic spontaneous imbibition in a micro-fluidic pore taken from a thin section of a Berea sandstone, as shown in

Figure 5. It can be observed that the decane imbibes from the bottom right corner and enters the nearest top right channel first. Again this is the nearest channel and not the one with the highest capillary entry pressure. This result supports our earlier observations: for the case of dynamic imbibition, the local geometry of the network model junction determines the filling sequence, rather than the capillary entry pressure of the channels.

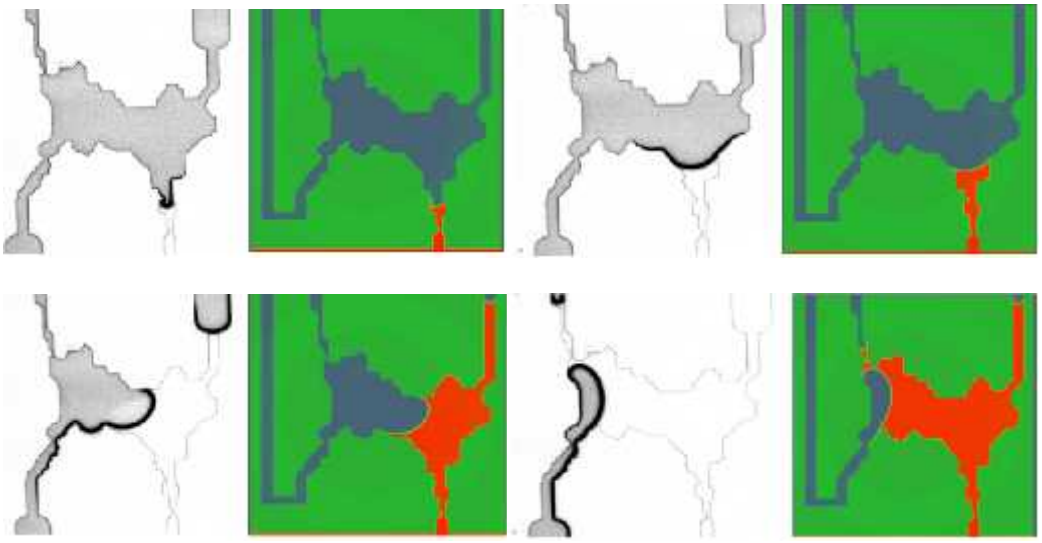

Figure 5: Snapshots of dynamic spontaneous imbibition of decane in a Berea sandstone micro-model

LB SIMULATIONS IN PORE SPACE IMAGES

In the above, we have validated that the detailed displacement mechanisms in single pore junctions observed in the micro-fluidic experiments, including static imbibition and drainage, snap-off and dynamic imbibition, are well matched by the LB simulations. This lends credibility to the accuracy of the simulations. Therefore we extend our calculations to multi-pore displacements in digital pore space images of real rock samples. Here we consider a pore space image of a Bentheimer sandstone, obtained from micro-CT scanning experiments, having a sample size of (512 x 256 x 256) voxels, resolution 4.9 μm and porosity 0.234. The single phase permeability is 4755 mD, determined from LB calculations. For more details, we refer to [10]. We present the pore space image and single phase flow field [10] in Figure **6**.

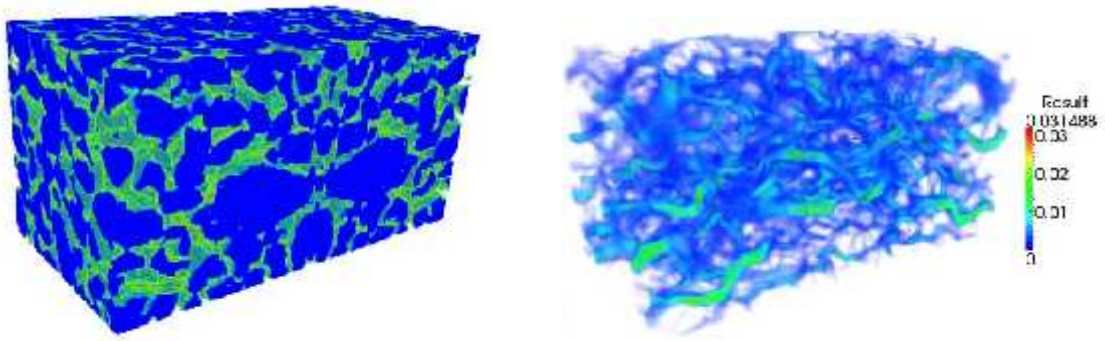

Figure 6: Pore space image (left; pore is green, solid is blue) and velocity distributions (right) of Bentheimer sandstone sample; red and blue indicate high and low velocities respectively.

First, we numerically measure the capillary pressure curve for the Bentheimer sandstone

using our LB code. A drainage process is simulated to mimic the experimental configuration. A buffer layer of 10 lattice sites wide is added at the inlet of the sample for injecting non-wetting phase. A porous plate is added at the outlet of the sample to prevent the non-wetting phase flowing out. This configuration is consistent with the experimental setup. The system is mirrored in the direction of the flow (z-axis), and then periodic boundary conditions are used. A constant colour boundary condition, which converts all entry fluid into non-wetting, is applied for the inlet. This guarantees that the wetting phase sticks to the rock surface and leaves the non-wetting phase in the center of the pore/throat. We note that advanced boundary conditions, such as constant pressure / flux and inlet colour boundary conditions based on wetting/non-wetting phase distributions, have been proposed. In this paper we use periodic and constant colour boundary conditions for reasons of simplicity and numerical stability. The static contact angle is set to 30°, which is consistent with oil-water contact angles in water-wet rocks [11]. A pressure gradient ΔP is applied to both phases until the system reaches steady state as the saturation equilibrates. Then one point on the capillary pressure curve is obtained. More points on the curve are obtained by applying different ΔP. The calculated capillary pressure is converted into the dimensionless Leverett-J-function:

$$J(s) = \frac{P_c}{\sigma \cos\theta}\sqrt{\frac{\kappa}{\varphi}} \quad (4)$$

where P_c is capillary pressure, κ absolute permeability, φ the porosity, σ surface tension, θ contact angle. The comparison of computed and measured [11] capillary pressure curve is shown in Figure 7. The agreement between the experimental measurement and simulation is generally good. The predicted irreducible wetting phase saturation (Swi = 7%) is similar to the experimental measurement. However, the calculated capillary pressure for this saturation is significantly lower than the experimental data. This may be due to resolution effects: small pores or throats may not be captured by micro-CT imaging. Such pores or throats are also difficult for LB simulation. These pore sizes or throat sizes may be smaller than the interfacial width in the LB simulation and therefore high capillary pressure may lead to poor numerical stability. These difficulties may be overcome using high resolution, although this will increase the computional cost.

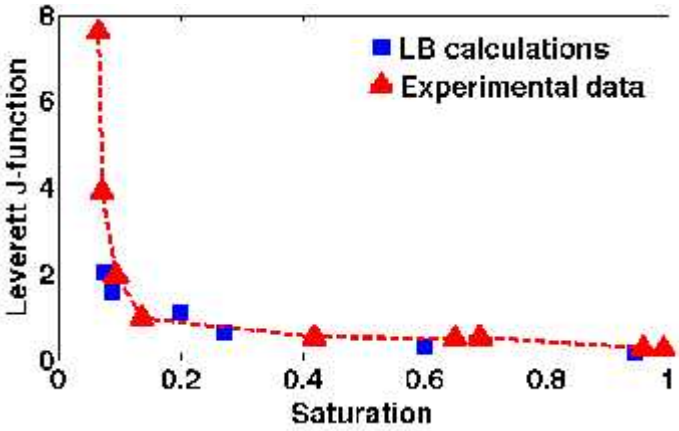

Figure 7: Computed capillary pressure (blue) in comparison with experimental results (red) ([11]) for Bentheimer sandstone.

As an example of multi-pore displacement, we show snapshots of the drainage process of Bentheimer sandstones in Figure **8**. From these figures, we observe that the big pores and channels are filled with non-wetting phase first, due to low capillary pressure. Small pores and throats are not filled with non-wetting phase due to the high capillary pressure. The fluid in these pores becomes residual wetting phase that cannot be drained out, unless a further increase of injection pressure is applied.

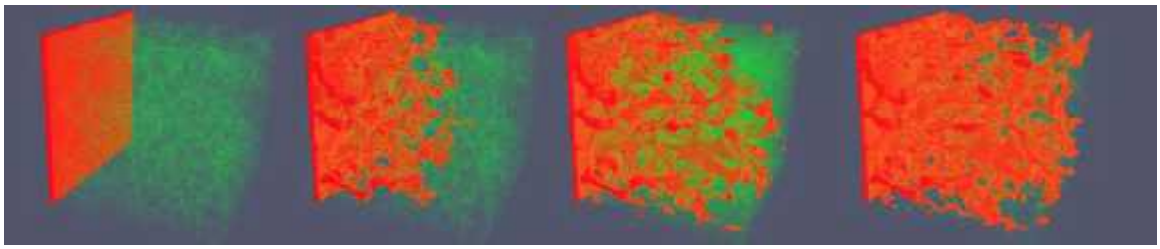

Figure 8: Snapshots of drainage process simulation of Bentheimer sandstone. The non-wetting phase is shown in red and the rock is shown in transparent green. Saturation increases from left to right.

Finally, we calculate relative permeabilities for our rock sample. There are a few studies in the open literature on the direct calculation of relative permeability of reservoir rocks [11, 12, 13]. The calculation requires a high level of accuracy, reliability and efficiency of the algorithm. It is also very difficult to reproduce the experimental conditions in the simulations. The papers cited above report calculation of the relative permeability based on random distribution of the non-wetting phase according to the desired saturation. This initial configuration is easy to set up but has a number of disadvantages: 1) it does not recover the experimental measurement procedures; 2) small or dead pores may be occupied by the nonwetting phase, which is not the case in the experiments due to high capillary pressure; 3) it is difficult to calculate the imbibition relative permeability curve due to lack of drainage-imbibition hysteresis. For this reason, we have developed a

process-based approach for the initial non-wetting phase distribution, based on imbibition simulations as a starting point for subsequent drainage calculations. For details of this method, we refer to [14]. In this fashion, we calculate relative permeability curves for both drainage and imbibition. These curves are shown in Figure **9**.

We observe that the agreement with experimental data is generally good for both drainage and imbibition. However, the non-wetting phase relative permeability is slightly over-predicted at high wetting phase saturations for both drainage and imbibition calculations. The relative permeability end point for imbibition is also over-predicted by the LB simulation. These discrepancies may be due to 1) periodic boundary conditions used: advanced constant pressure / flux boundaries may reflect experiment more accurately; 2) limited resolution of the mesh in small pores and throats, as the thin wetting layers (with a thickness smaller than the imaging resolution) near the rock surfaces and small scale snapped-off NWP bubbles may not be captured effectively [6]. A potential solution is to use a finer mesh, although this will decrease the computational efficiency. We are currently working on an efficient GPU implementation of the code to solve these problems.

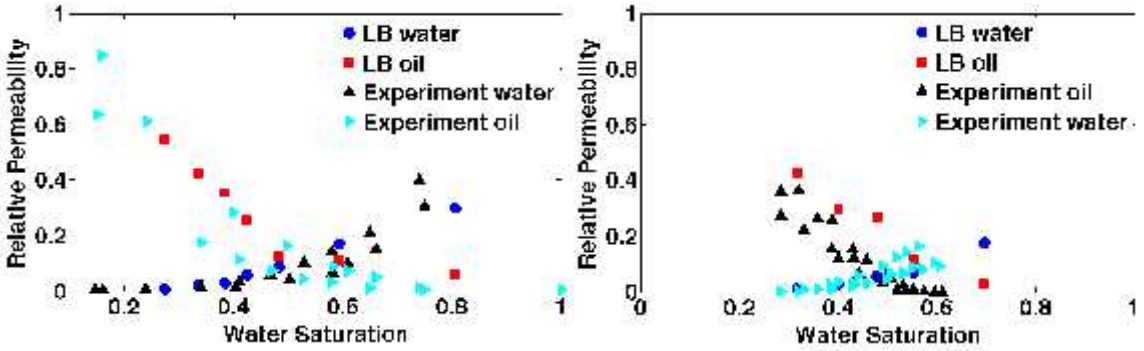

Figure 9: Steady-state relative permeability simulation for drainage (left) and imbibition (right) in direct comparison with experimental data (Ramstad et al., 2012) for Bentheimer sandstone.

CONCLUSIONS AND DISCUSSION

We have investigated displacement mechanisms of immiscible fluids in micro-fluidic models with designs ranging from simple pore junctions to a pore from a Berea sandstone thin-section. For this purpose, we have developed a lattice-Boltzmann (LB) model to study the multi-phase flow processes in comparison with experimental results in purpose-built micro-fluidic geometries. In this paper, have focused on the LB simulations, in direct comparison with the experiments. First, we have studied quasi-static drainage and imbibition processes in single junctions, including snap-off, and observe good agreement with Young-Laplace capillary filling rules. However, for larger capillary pressure drops, often associated with the process of spontaneous imbibition where the pressure drop

cannot be controlled, we observe that the sequence of pore filling is determined by local pore geometry rather than the Young-Laplace law. The LB simulation results are in good agreement with the micro-fluidic experimental observations. We extend our simulations to multi-pore immiscible displacement in rock cores and observe capillary pressure and relative permeability in reasonable agreement with experiment.

ACKNOWLEDGEMENTS

We gratefully acknowledge funding from the Qatar Carbonates and Carbon Storage Research Centre (QCCSRC), provided jointly by Qatar Petroleum, Shell and Qatar Science and Technology Park. EMC also acknowledges the UK Engineering and Physical Sciences Research Council (EPSRC) for funding.

REFERENCES

[1] Lenormand, R.; Zarcone, C. & Sarr, A., "Mechanisms of the Displacement of One Fluid by Another in a Network of Capillary Ducts", *J. Fluid Mech.* (1983), **135**, 337–353.

[2] Roof, J.R., "Snap-off of oil droplets in water-wet pores", *SPE Journal* (1970), **10**, 1, 85–90.

[3] Boek, E.S. & Venturoli, M. "Lattice-Boltzmann studies of fluid flow in porous media with realistic rock geometries", *Computers and Mathematics with Applications* (2010), **59**, 2305-2314.

[4] Chapman, E.; Yang, J.; Crawshaw, J.P & Boek, E.S., "Pore scale models for imbibition of CO_2 and analogue fluids in etched micro-model junctions using micro-fluidic experiments and direct flow calculations", *Energy Procedia* (2013), **37**, 3680-3686.

[5] Chapman, E.; Yang, J.; Crawshaw, J.P & Boek, E.S., "Pore Filling Events in Single Junction Micro-Models with Corresponding Lattice Boltzmann Simulations", manuscript under review (2014).

[6] Yang, J. & Boek, E.S., "A comparison study of multi-component lattice-Boltzmann models for flow in porous media applications", *Computers and Mathematics with Applications* (2013), **65**, 882-890.

[7] Ahrenholz, B., Tölke, J., Lehmann, P., Peters, A., Kaestner, A., Krafczyk, M., & Durner, W. "Prediction of capillary hysteresis in a porous material using lattice-Boltzmann methods and comparison to experimental data and a morphological pore network model", *Adv. Water Resour.* (2008), **31**(9), 1151–1173.

[8] Tolke, J. "LB simulations of binary fluid flow through porous media", *Phil. Trans. R. Soc. Lond. A* (2002), **360**, 535.

[9] Buick, J.M. & Greated, C.A. "Gravity in a lattice Boltzmann model", *Phys. Rev. E* **(**2000), **61**, 5307.

[10] Yang, J.; Crawshaw, J.P. & Boek, E.S. "Quantitative determination of molecular propagator distributions for solute transport in homogeneous and heterogeneous porous media using LB simulations", *Water Resources Research* (2013), **49**, 8531-8538.

[11] Ramstad, T., Idowu, N., Nardi, C., & Øren, P. E. "Relative permeability calculations from two-phase flow simulations directly on digital images of porous rocks", *Transport Porous Med*. (2012), **94**, 487–504.

[12] Pan, C., Luo, L.-S. & Miller, C. T. "An evaluation of lattice Boltzmann schemes for porous medium flow simulation", *Comput. Fluids* (2006), **35**, 898–909.

[13] Koroteev, D., Dinariev, O., Evseev, N., Klemin, D., Nadeev, A., Safonov, S., & de Jong, H. "Direct Hydrodynamic Simulation of Multiphase Flow in Porous Rock", *SCA2013-014*.

[14] Yang, J. & Boek, E.S. "LB simulation of immiscible fluid flow in reservoir rocks", manuscript in preparation (2014).